J Paleolimnol (2008) 40:963–985
DOI 10.1007/s10933-008-9210-x

ORIGINAL PAPER

Limnological and sedimentary processes at Sawtooth Lake, Canadian High Arctic, and their influence on varve formation

Pierre Francus · Raymond S. Bradley · Ted Lewis · Mark Abbott · Mike Retelle · Joseph S. Stoner

Received: 24 May 2007 / Accepted: 30 March 2008 / Published online: 14 May 2008

Abstract This paper synthesizes data collected to document the modern limnological and sedimentary processes in South Sawtooth Lake located on northern Ellesmere Island, Nunavut, Canada. Field observations show that the finely laminated sediments deposited in the distal basin are formed by the settling of overflows and interflows, and in rare occasions, by non-erosive hyperconcentrated density flows. Thin-sections of these sediments allowed for the classification of the sedimentary fabrics into six facies, each representing different limnological processes. The sediments in this distal basin are considered to be continuous and annually laminated (varved) based on radioisotope analyses, and both limnological and sedimentological evidence.

Keywords Varves · Physical limnology · Image analysis · Thin-section · Sedimentary processes · Paleoclimate

Introduction

A number of lakes containing laminated sediments were identified as part of an effort aimed at retrieving high-resolution paleoclimate records from lake sediments in the High Arctic (Lamoureux and Bradley

P. Francus · R. S. Bradley · T. Lewis · M. Abbott
Department of Geosciences, Climate System Research Center, University of Massachusetts, Amherst, MA 01003, USA

R. S. Bradley
e-mail: rbradley@geo.umass.edu

T. Lewis
e-mail: lewist@geo.umass.edu

P. Francus (✉)
Centre Eau, Terre et Environnement, Institut National de la Recherche Scientifique, Québec, Québec, Canada G1K 9A9
e-mail: pfrancus@ete.inrs.ca

P. Francus
GEOTOP-UQAM-McGill, Montréal, Québec, Canada H3C 3P8

M. Abbott
Department of Geology and Planetary Science, University of Pittsburgh, Pittsburgh, PA 15260, USA
e-mail: mabbott1@pitt.edu

M. Retelle
Department of Geology, Bates College, Lewiston, ME 04240, USA
e-mail: mretelle@bates.edu

J. S. Stoner
College of Oceanic and Atmosphere Sciences, Oregon State University, Corvallis, OR, USA
e-mail: jstoner@coas.oregonstate.edu

1996; Francus et al. 2002; Smith et al. 2004). Chronology and identification of the climatic signal in the sediments are critical for paleoclimate reconstructions. In varved sediments the annual deposition of layers provides the chronology given that there are no missing sections due to erosion or periods of non-deposition. Calibration of the hydroclimatic signal recorded in varved sediment is necessary to provide quantitative reconstructions of past conditions (e.g., Olhendorf et al. 1997; Blass et al. 2007). Integrated monitoring approaches are necessary (Hodder et al. 2007), but rarely done in the Arctic (e.g., Hambley and Lamoureux 2006 and references therein). Calibration of the climate signal is much more problematic in the High Arctic as there are very few meteorological stations and they are restricted to low-elevation coastal locations that may not be fully representative of the environments where the lakes are located. For this reason, we investigated the processes involved in sediment transport to each of the lakes, and examined changes in inter- and intra-annual physical limnology to better understand the within-lake sediment transport processes (Hardy et al. 1996; Retelle and Child 1996; Braun et al. 2000; Lewis et al. 2005). In parallel, we analyzed the sedimentary facies quantitatively at the microscopic scale using an image analysis technique applied to backscattered electron (BSE) images of thin-sections in order to infer their mode of deposition from their textural and structural characteristics (Francus 1998; Francus and Karabanov 2000). Together with the limnological measurements, these investigations provide a mechanistic basis for interpreting records and complement empirical statistical calibrations. Here, we report on studies of varved sediments in South Sawtooth Lake (79.3°N, 83.9°W, 280 m asl). Our previous work at South Sawtooth Lake noted the presence of a varved sedimentary sequence and linked the nival component of the varves with snowmelt intensity (Francus et al. 2002). We also documented the rapid colonization of diatoms and development of a diverse diatom assemblage in the lake starting ~1920 (Perren et al. 2003), and showed that most of the sediment transfer from the single tributary into the lake occurs as a result of snowmelt runoff (Lewis et al. 2005). In this paper, we synthesize and complement the previously published information with unpublished data (Patridge 1999) and new results aiming to understand the processes that lead to varve formation.

Study area

South Sawtooth Lake (unofficial name) is located on the Fosheim Peninsula, Ellesmere Island, Nunavut, Canada (Fig. 1). The lake is the highest of three lakes situated in the Sawtooth Mountain range. South Sawtooth Lake is elongated in shape and divided into a proximal and a distal basin (100 and 80 m deep, respectively) separated by a 60-m deep sill. The lake surface area is about 2.6 km^2 and its watershed, entirely above marine limit, has an area of 47 km^2 with a maximum elevation of ~915 m asl. South Sawtooth Lake is surrounded by the steep walls of a col within the Sawtooth Range (Fig. 2). A single tributary feeds the lake from the southeast, while the outlet is located at the northwestern end (Fig. 1). The watershed is currently not glacierized. Bedrock lithology varies across the watershed. In the Wolfe valley to the east of the lake, where the main inflow is located, the Tertiary Eureka Sound Formation makes up the majority of the outcrops. The prominent lithologies consist of poorly consolidated sandstones interstratified with siltstones, and shales, with minor amounts of coal. The rocks in direct contact with the lake that are located in the col within the Sawtooth Range, are made of harder and older rocks from the Triassic—the Bjorne and the Schei Point Formations—mainly sandstones and calcareous siltstones, with minor amounts of limestones and shales (Geological Survey of Canada 1972). Blanket and veneer tills provide evidence of a formerly extensive ice cover on the Fosheim Peninsula (Dawes and Christie 1991; Bell 1996; Ó Cofaigh 1999), although it seems that this site became ice-free between 8,000 and 5,000 years BP (Ó Cofaigh et al. 2000).

The summer climate in the area is relatively warm with temperatures above freezing because of the continentality of the Eureka Sound intermontane region (Edlund and Alt 1989). The surrounding mountains and highlands limit the incursion of cold Arctic Ocean air masses and cyclonic activity from Baffin Bay (Edlund and Alt 1989), and promote a foehn effect over the area. From 1947 to 2001 AD, the average monthly air temperatures in June, July, and August at Eureka, the closest Meteorological Service of Canada station (84 km NW; 10 m asl; Fig. 1), were 2.2, 5.5, and 3.1°C, respectively; all other monthly mean air temperatures were below freezing. The area is an extreme polar desert where annual precipitation, which falls mainly as snow, averages 68 mm, making it the driest place in

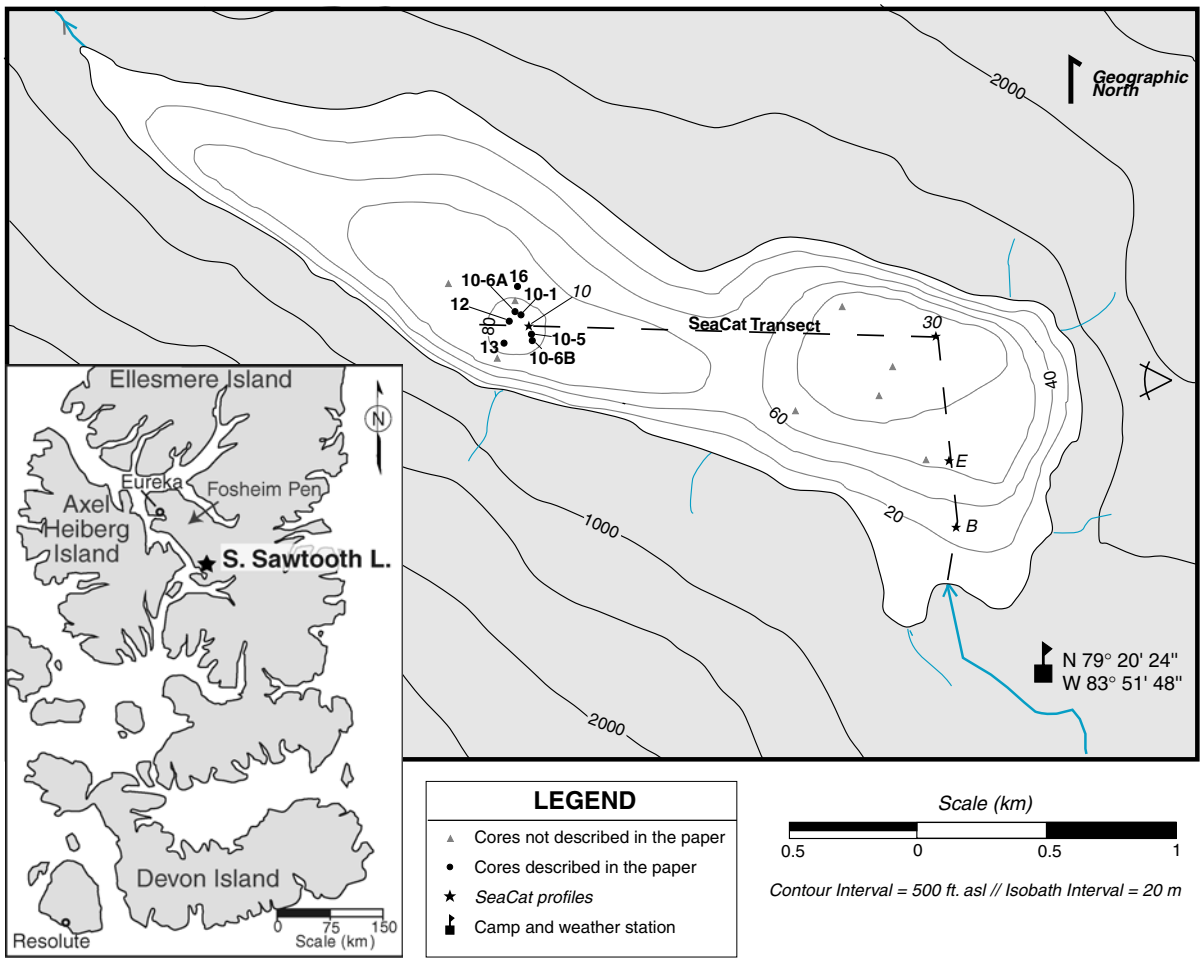

Fig. 1 Map of South Sawtooth Lake showing the location of sediment cores, transects of limnological measurements, and weather station data. Bathymetry is inferred from 32 manual measurements through drill holes from the ice surface. The view symbol indicates the location of photograph A in Fig. 2

Canada (Environment Canada 2003). Average annual rainfall is 25 mm; mean June, July, and August rainfall totals are 3.7, 11.2, and 8.8 mm, respectively. The relatively high summer temperatures combined with limited cloudiness produce more melting days and longer snow-free periods and favor high diversity and density of vascular plants (Garneau and Alt 2000). The catchment is largely unvegetated: the lowlands support an enriched prostrate shrub flora (Edlund and Alt 1989) whereas the felsenmeer highlands support only a sparse saxifrage-dominated community.

Methods

We conducted field work at South Sawtooth Lake during the summers of 1998, 1999, 2000, and 2006.

Meteorology and hydrology

The weather and hydrology of the input stream were monitored simultaneously only during summer 1998 with the methods and results described in detail by Lewis et al. (2005). Air temperature was measured at the camp (Fig. 1) with a Vaiasala HMP45C sensor protected from solar radiation inside a 12-plate Gill shield. Measurements obtained every minute were stored as hourly averages on a Campbell Scientific Inc (CSI) datalogger. An unshielded cylindrical precipitation gauge, precise to 0.254 mm, and graduated to 0.2 mm, was placed on the ground, and read several times daily during the 1998 field season (Lewis et al. 2005). Water conductivity and temperature were measured every 10 s using a CSI 247

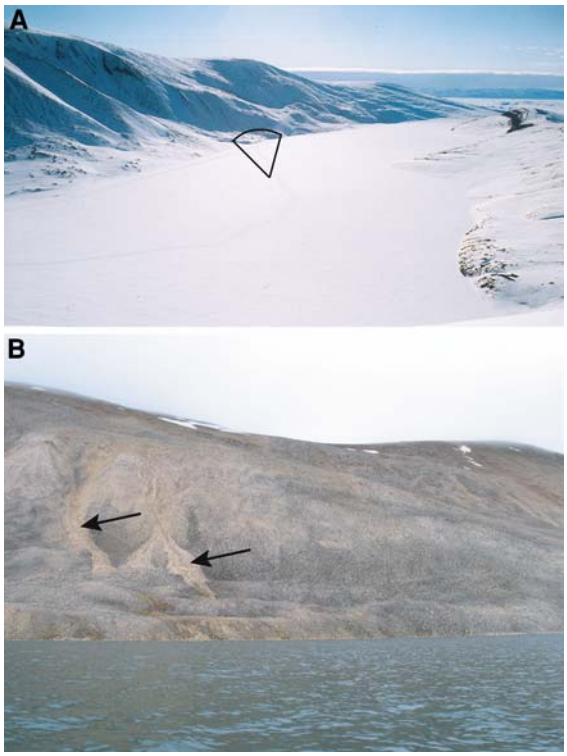

Fig. 2 (**a**) Photograph of South Sawtooth Lake from the eastern side looking towards the west showing the steep slopes near the distal basin. The proximal basin is in the foreground and Axel Heiberg Island is in the background. The view symbol indicates the location and direction of (**b**). (**b**) View of a recent aerial debris flow (lighter shades) on the southern slope of South Sawtooth Lake highlighting active erosional processes on the slopes surrounding the distal basin. Arrows point to debris flow deposits. Photograph by Mark Besonen

probe (Lewis et al. 2005). Stage was measured between 12 June and 17 July with two Geokon Model 4850 vibrating wire pressure transducers interfaced with the datalogger. One transducer was inside a 5.1-cm diameter slotted stilling well, and the other measured air pressure changes (Lewis et al. 2005). Stream velocity was measured with a Swoffer Model 2100 flow meter (precision ±1% from 0.03 to 7.50 m s^{-1}). Discharge measurements were performed manually at 60% of the stream depth using standard measurement techniques (cf. Hardy 1995). Suspended sediment samples were manually obtained near the thalweg using a US DH-48 depth-integrating sampler. Suspended sediment concentration (SSC) was also automatically recorded using a D&A Instruments OBS-3 infrared backscatterance unit interfaced with the CR10 datalogger (Lewis et al. 2005).

Modern limnology

The water column was monitored using a *SeaCat profiler SBE 19 CTD* from Sea-bird Electronics (called hereafter "SeaCat") during the 1998 summer season. Daily SeaCat profiles were obtained from 30 May (Julian Day 150) through 15 July (JD 196) at 4 stations along a proximal to distal transect (Fig. 1) (Patridge 1999). Four additional profiles were obtained during the 2000 field season with the same instrument. The SeaCat automatically records water depth, water temperature, salinity, dissolved oxygen, and light transmission at 0.5-s intervals as the instrument is lowered through the water column. In August 2006, we obtained one profile with a Hydrolab MiniSonde/Surveyor 4a combination when the lake was ice-free.

The SeaCat was interfaced with a Sea Tech transmissometer. Calibration of the transmissometer to SSC was carried out in the laboratory by preparing a sediment/water slurry of sonicated South Sawtooth Lake sediment. Subsamples of the slurry were added to a continually mixed bath. SSC of the bath was determined by vacuum filtration of hand-dipped aliquots using standard techniques (Hardy 1996). This method provided a calibration of the transmissivity data to SSC for the most turbid conditions. However, because of the fine-grained nature of the sediment, it was difficult to produce relatively clear calibration samples with a transmissivity of ~45–90%. Therefore, the lab calibration was supplemented with data collected in situ with the same instrument, at Lake Tuborg (80.98°N, 75.55°W), a nearby lake on Ellesmere Island with similar sediment properties. Van Dorn water samples were obtained, and SSC was determined in the same way as noted above (Lewis et al. 2007). The two data sets compare well where data overlap (Fig. 3), probably because particle size distributions in subaqueous sediment plumes are broadly similar in both lakes (Gilbert et al. 1997; Gilbert and Butler 2004). The best-fit curve shown in Fig. 3 was obtained for the composite data set, and transmissivity data (x) were transformed into SSC (y) using this equation:

$$y = 8.1242 + (-1.4822 \ln x)^2. \quad (1)$$

Salinity is reported as parts per thousand (PPT). Potential density anomaly (σ_θ) was calculated using

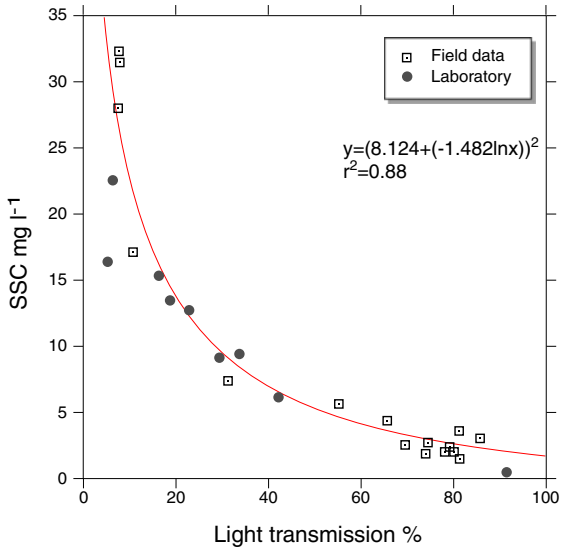

Fig. 3 Light transmission measured by the SeaCat and corresponding SSC measured in the laboratory (gray circles) and in the field (open squares). The best-fit curve is Eq. (1)

depth, temperature, and salinity (JPOTS Editorial panel 1991), and was adjusted for the atmospheric pressure using the mean summer 1998 pressure recorded at the South Sawtooth Lake weather station (0.969 atm).

Sediment Cores

We retrieved a total of 31 sediment cores from different areas of the proximal and distal lake basins (Fig. 1) using the following coring techniques. (1) Short gravity cores were recovered using a Glew coring system with a 7-cm-diameter barrel (Glew et al. 2001). These cores were up to 60 cm long (but typically ~30 cm) with an almost undisturbed water-sediment interface. (2) Freeze cores were retrieved using aluminum wedges weighted with lead and filled with a mixture of dry ice and methanol (Glew et al. 2001). (3) Longer cores were taken using a submersible Rossfelder VT-1 vibracoring system with 10-cm core barrels. These cores were typically 4.5–5 m long, but the top ~10 cm were generally disturbed. The majority of the cores were retrieved from the distal basin because of the presence of undisturbed laminated sediments. Sediment facies were described according Schnurrenberger et al. (2003).

Laboratory work

Non-destructive analyses

High-resolution images were obtained from split cores under a light table. Magnetic measurements were made on u-channel samples in Paleomagnetism Laboratories at the University of California, Davis and the University of Florida. An anhysteretic remanent magnetization (ARM) was applied to four vibracores and one Glew core from South Sawtooth Lake using a 100 mT peak alternating field (AF) and a 0.05 mT direct current biasing field. The ARMs were measured, then re-measured at 1-cm spacing after stepwise AF demagnetization at 5 mT steps up to 80 mT.

Destructive analyses

We made thin-sections using the method described in Francus and Asikainen (2001). Aluminum trays filled with sediment removed from the core were shock frozen in liquid nitrogen and freeze dried. The trays were then impregnated using the low viscosity Spurr's epoxy resin (Lamoureux 1994) and thin-sections were cut from the impregnated samples. Thin-sections were scanned using a flat bed scanner with transparency capabilities (Agfa Duoscan) at 1,440 dpi resolution. The pixel size was 17 μm. For each thin-section, two scans were performed. The first used the regular light of the device. The second used two polarized filters at 90°, sandwiching the thin-section between the filters, to produce crossed-polarized light (Lamoureux and Bollmann 2004). Thin-sections were also viewed using JEOL JSM-5410 and Zeiss 50XVP scanning electron microscopes (SEM) in BSE mode (Soreghan and Francus 2004). Image analysis techniques were applied to SEM images in BSE mode according to Francus (1998). The equivalent disk diameter of each detected grain (Francus et al. 2002) was measured and used to calculate the weight of 46 size classes from 0.5 to 2,000 μm to estimate the grain-size distribution of the individual units. Standard grain-size parameters were calculated with the Gradistat software (Blott and Pye 2001) that uses linear interpolation to calculate statistical parameters according to Folk and Ward's (1957) graphical method and derived physical descriptions are reported in Table 1.

Table 1 Size measurements of the image presented in Fig. 10 using image analysis techniques outlined in Francus (1998) and used in Francus et al. (2002). The minimum size of detected objects is 3 μm. Equivalent disk diameter was calculated for each grain, then the weights of 46 size classes from 0.5 to 2,000 μm on a log scale were calculated assuming spherical objects of quartz density. Standard grain-size parameters were calculated using Gradistat software (Blott and Pye 2001)

Grain-size class	Facies 1	Facies 3	Facies 3 sand layer only	Facies 4 silt layer below graded bed	Facies 4 graded bed lower half	Facies 4 graded bed upper half	Facies 6 disturbed bed
V fine sand	0.0%	7.1%	10.0%	0.0%	1.3%	0.0%	3.2%
V coarse silt	0.0%	35.7%	46.5%	1.8%	19.5%	2.7%	43.0%
Coarse silt	17.7%	26.0%	27.6%	38.5%	54.5%	41.1%	36.7%
Medium silt	44.4%	16.8%	10.9%	48.5%	21.7%	43.2%	13.5%
Fine silt	35.6%	13.4%	4.6%	11.0%	2.8%	12.2%	3.3%
V fine silt	2.2%	1.1%	0.4%	0.3%	0.1%	0.8%	0.2%
Grain-size statistics (geometric μm)*							
Mean ($\bar{x}$)	9.380	22.530	31.690	12.750	21.200	13.800	28.120
Sorting (σ)	1.657	2.320	1.917	1.497	1.621	1.591	1.802
Skewness (Sk)	0.096	−0.292	−0.296	−0.144	−0.022	−0.147	−0.202
Kurtosis (K)	0.991	0.815	1.016	0.990	1.070	0.931	0.908
Description*	Medium silt, moderately sorted, symmetrical, mesokurtic	Coarse silt, poorly sorted, fine skewed, platykurtic	V. coarse silt, moderately sorted, fine skewed, mesokurtic	Medium silt, moderately sorted, fine skewed, mesokurtic	Coarse silt, moderately well sorted, symetrical, mesokurtic	Medium silt, moderately well sorted, fine skewed, mesokurtic	Coarse silt, moderately sorted, fine skewed, mesokurtic

* After Folk and Ward (1957)

Results

Climate, hydrology, and sediment delivery

Lewis et al. (2005) reported and discussed the climatic and hydrological data sets acquired from the inlet stream at South Sawtooth Lake during the summer of 1998. Here we report only a subset of these previously published results that are relevant to our discussion. Figure 4 presents climate data (mean daily air temperature, thawing degree day, and daily precipitation), hourly SSC measured in the South Sawtooth Lake River, and the discharge and daily mean temperature of the stream. Lewis et al. (2005) showed that most of the sediment is delivered to South Sawtooth Lake during the early snowmelt season. However, in 1998, a significant volume of sediment was delivered by an extreme suspended sediment pulse, and to a lesser extent, by summer rainfall events. The total amount of fluvial sediment delivered by the river during the 1998 field season was 1,561 tons or 0.033 kg m^{-2}. Streamflow began on the ice and snow-covered surface on 2 June (JD153), and a diurnal cycle was visible in the stream discharge and SSC shortly afterward. At the beginning of the snowmelt period, discharge rose to its annual peak of 4 m^3 s^{-1} and remained high for about 9 days, then decreased to values lower than 2 m^3 s^{-1} for the rest of the season, even after small rainfall events (Lewis et al. 2005). About 28% of the total sediment yield occurred between 2 June (JD153) and 11 June (JD162), when the stream water temperature remained below 1.3°C, i.e., the daily mean lake water temperature.

Lake physical properties

Lake temperature

Lake temperature profiles at site 10 during the 1998 field season (Fig. 5) displayed inverse thermal-stratification with a mean temperature of 1.1°C at 3 m depth increasing to 2.1°C at the bottom of the lake at the beginning of the season (30 May; JD150). Mean temperature at site 10 increased progressively throughout the study period (30 May–5 July;

JD150–JD186). This temperature increase led to the collapse of thermal stratification, as mean temperatures at all sites on JD186 (5 July) were 2.1°C at 3 m depth, and 2.2°C at the lake bottom.

The structure of the temperature profile acquired at site 10 on 10 June 2000 (JD161) was similar to the one obtained 2 years earlier (Fig. 5a, b): lake temperatures were close to 0°C at the surface, and

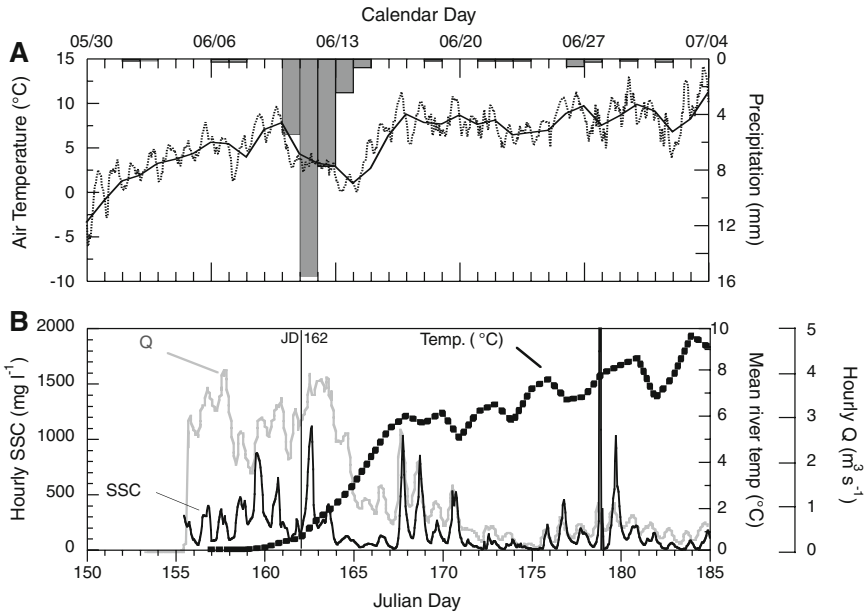

Fig. 4 (**a**) Hourly and mean daily air temperature, thawing degree days and daily precipitation (inverted y-axis). (**b**) Hourly river discharge (Q), daily stream temperature and hourly measured SSC. Redrawn from Lewis et al. (2005)

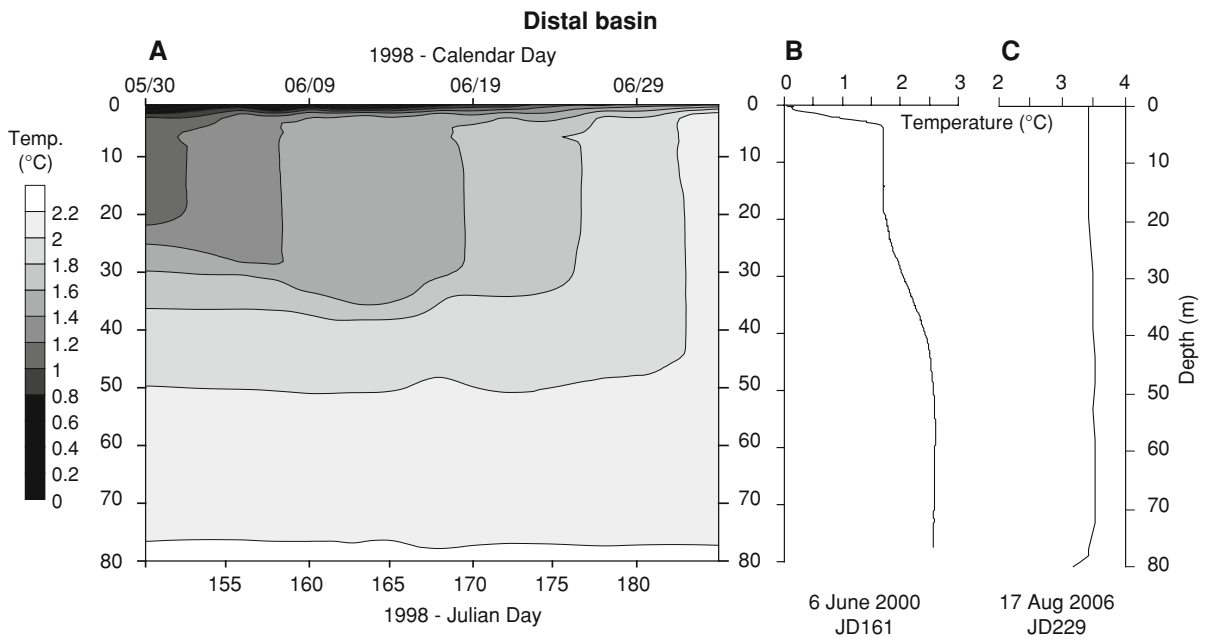

Fig. 5 Selected South Sawtooth Lake water temperature profiles at distal site 10. (**a**) Contour plot of measurements acquired in 1998 using the SeaCat. (**b**) Profile for JD 161 (10 June) acquired in 2000 using the SeaCat. (**c**) Profile for JD 229 (17 August) acquired in 2006 using the Hydrolab

increased abruptly to 1.7°C at 4 m depth. Below that, the temperature increased steadily to reach a maximum of 2.6°C at 52 m depth (Fig. 5b). Three other profiles (not shown) taken in June 2000 in the proximal and distal basins have similar structures to those acquired 2 years earlier. Finally, a Hydrolab profile, obtained in mid-August 2006 when the lake was ice-free, revealed an isothermal water column at 3.4°C, with the exception of the lowermost 2 m where temperature was 3.1°C (Fig. 5c).

Dissolved oxygen, salinity, and potential density anomaly

In the proximal basin on 10 June 2000 (JD161), the oxygen content was about 10 mg l^{-1} in the epilimnion and decreased progressively to 6.2 mg l^{-1} in the hypolimnion (not shown here). The salinity was about 0.058 ppt in the epilimnion and slightly higher at the bottom, 0.062 ppt.

In the distal basin (Fig. 6), the salinity profile was very different. It showed relatively fresh water in the epilimnion, then reached a steady value of 0.06 ppt but started to increase again at 62 m depth, reaching a maximum of 0.08 ppt near the bottom (Fig. 6a). The potential density anomaly (σ_θ) increased in three steps, the first step occurring at about 5 m depth, the second between 24 and 40 m depth, and the last below 60 m depth. In June 2000, the oxygen profile of the distal basin mirrored salinity, with dissolved oxygen values starting to decrease toward the bottom around 62 m depth, reaching 4.5 mg l^{-1}. When the lake was ice free in 2006, the oxygen content of most of the water column was much higher than during ice-covered conditions in early June 2000. However, the bottommost 2 m continued to have extremely low dissolved oxygen. Differences between near-bottom dissolved oxygen content between casts shown in Fig. 6a, b are likely due to differences in instrumentation and methodology. Figure 6b shows a cast where the Hydrolab oxygen sensor was allowed to equilibrate for several minutes. Figure 6a cast is from the SeaCat, where it was allowed to descend at about 1 m s^{-1} through the water column.

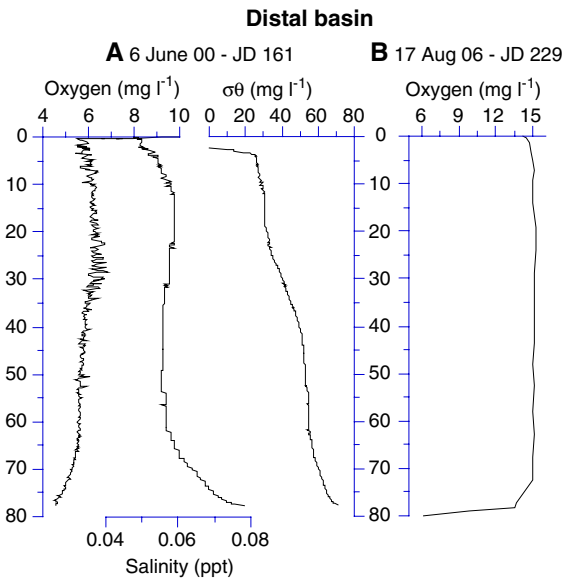

Fig. 6 (**a**) Dissolved oxygen, salinity, and potential density anomaly (σ_θ) at distal site 10 measured with the SeaCat on JD 161 (10 June) in 2000 in the distal basin (483 data points). (**b**) Dissolved oxygen on JD 229 (17 August) in 2006 measured with the Hydrolab (23 data points)

Lake SSC

Two snapshots of SSC along a transect across the lake, one for JD 162 (11 June) and a second for JD 183 (2 July) (out of the 16 measured during the 1998 field season) are presented in Fig. 7a, b, with transect locations shown in Fig. 1 (Patridge 1999). A time-series plot for site 10 in the distal basin is also shown (Fig. 7c). Discharge and fluvial SSC were low on JD 150 (30 May) with runoff initially under the frozen surface of the river. The inflowing 0°C stream water remained at the top of the warmer, yet denser, water column (Fig. 5a). On 7 June (JD158), the cold (0°C) stream water still moved as a hypopycnal flow with maximum SSC values up to 17 mg l^{-1} in the proximal basin, and reached the most distal sites. Simultaneously, the stream discharge reached its maximum (4 m^3 s^{-1}), but it did not carry much suspended sediment, less than 400 mg l^{-1} (Lewis et al. 2005). Beginning on JD162 (June 11) (Fig. 7a), the overflow plume became weaker, but a strong underflow, with SSC values reaching a maximum (>30 mg l^{-1}) started to develop as the SSC in the incoming stream reached 1,100 mg l^{-1}. After a period of lower temperature and reduced discharge, the stream temperature increased to 7.5°C on JD168 (17 June), the river discharge reached a maximum of 2.5 m^3 s^{-1} and the SSC 1,100 mg l^{-1} (Fig. 4). Once the stream water entered the lake, it flowed mainly as an underflow, but shifted to an interflow a couple of

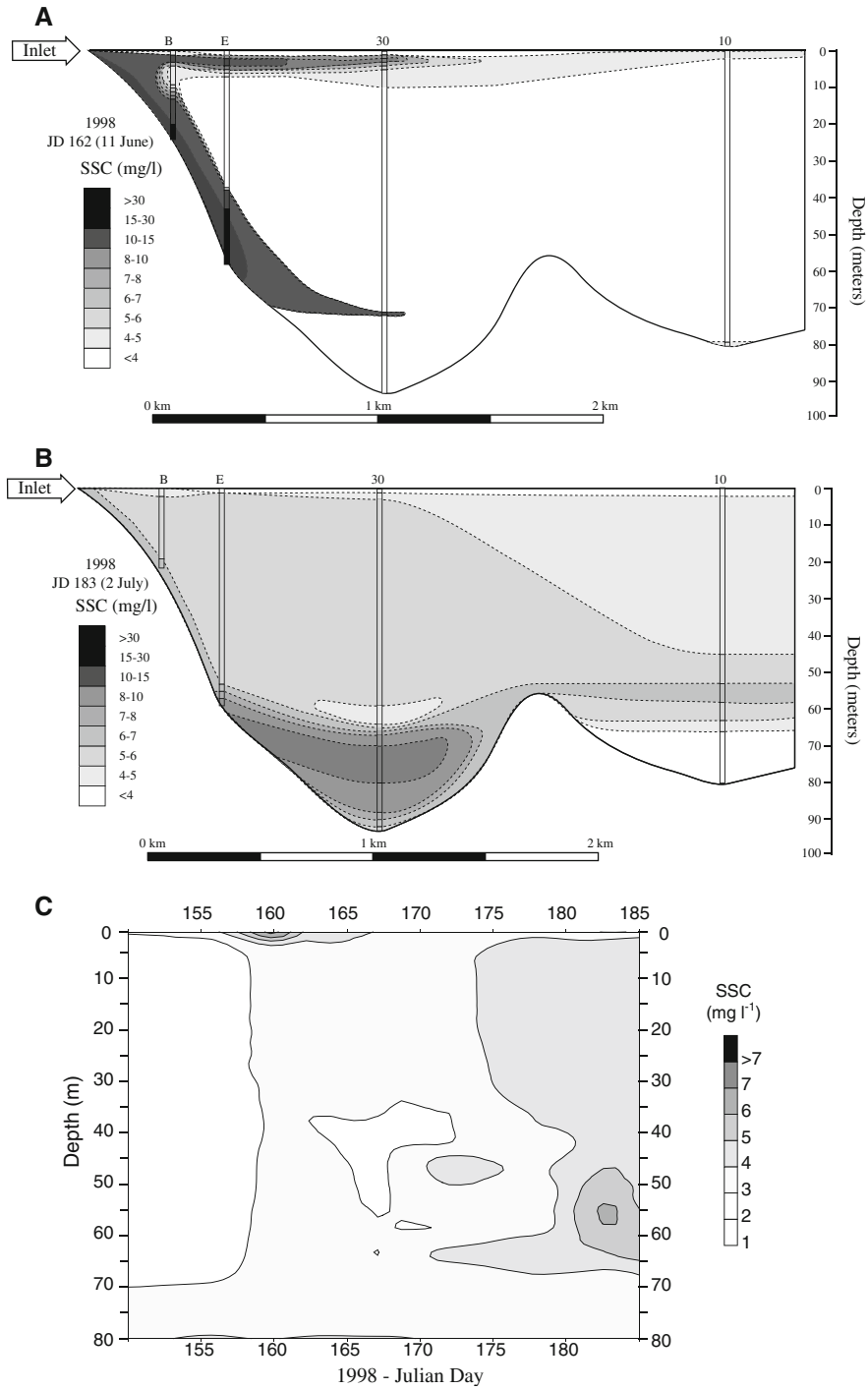

Fig. 7 SSC through space and time in 1998. Note the exponential scale of the SSC units. (**a**, **b**) SSC along a longitudinal transect across the lake going through four profiles, respectively, B, E, 30, 10 (location in Fig. 1) for Julian Day 162 (11 June) (A) and Julian Day 183 (2 July) (B). Plain contour lines are the measured profiles. Dashed contour lines between the profiles are interpolations drawn manually. (**c**) Temporal evolution of SSC from Julian Day 150 to JD 185 (30 May–4 July) at distal site 10. Profiles were interpolated with a Radial Basis interpolation using the software *Surfer*. Note that the scale is slightly different compared to those of the transects

days later on June 20–24 (JD 171–175) once it advanced further in the deep proximal basin (Fig. 7c). Finally, after a prominent SSC event in the stream (3,600 mg l^{-1}) that occurred June 27–29 (JD 179–181; Fig. 4), the flow reached the proximal deep basin on JD183 (2 July; Fig. 7b, c). The flow extended over the sill and continued as an interflow in the deep distal basin. Note that the input of sediments from overflows stopped as the SSC decreased in the few upper meters of the water

column (Fig. 7b, c). SSC at the distal site below 70 m (Fig. 7b) remained relatively constant, between 3 and 4 mg l^{-1}. This depth is reasonably coincident with the chemocline and pycnocline depth in the distal basin (Fig. 6). Two significant increases of SSC occurred in the lake during the season: SSC increased to >7 mg l^{-1} on JD160 (9 June) in the epilimnion and >6 mg l^{-1} on JD183 (2 July) at 56 m depth (Fig. 7c).

Sediment structure and lithology

The sedimentary sequence was succinctly described in Francus et al. (2002) and Perren et al. (2003) and was reported as varved based on radiogenic evidence and a preliminary laminae count. Here we present a comprehensive sedimentary description and additional evidence supporting the chronology and the varve interpretation.

Macroscopic description

Macroscopically, all sediment cores recovered from South Sawtooth Lake range from thinly laminated to thinly bedded. Each bed (defined as being >1 cm in thickness) and lamina (defined as being <1 cm in thickness) consists of a couplet with a basal silt to fine sand layer that grades into a clay-rich layer. The color of the sediment is mainly controlled by grain-size, from very dark brown (10YR 2/2) for the coarser units to lighter colors (very dark grayish brown; 2.5Y 3/2) for the clay-rich parts and shades of dark olive brown (2.5Y 3/3).

In the cores from the proximal basin, thin-beds (~5 cm) are common and all laminae are thicker than 1 mm. Some erosional features, such as unconformable contacts, are visible. In the distal basin, coarse beds are less frequent than in the proximal basin and are only 1 cm thick on average.

Correlations between cores

High-resolution images were used to correlate cores from different locations within the lake. The coarsest beds are easily matched between the proximal and the distal basin. Stratigraphic matches between cores within the distal basin are readily visible macroscopically in the magnetic grain-size data (Fig. 8).

High-resolution flat bed scans of thin-sections were used to correlate short and long cores from the distal basin at a microscopic scale. In the deepest area of the distal basin, laminae <1 mm are very frequent and well preserved, hence correlations between cores from the deep distal basin, i.e., from >80 m depth, are very good. Thin-sections cut from the uppermost sediments retrieved from gravity and vibracores have identical stratigraphies (Fig. 9a). However, the thinnest visible laminae progressively fade away in cores from sites with decreasing water depth. Indeed, the finely laminated pattern visible in the sediment core from the very deepest part of the distal basin, i.e., 81.3 m depth, cannot be distinguished in cores from shallower locations, i.e., 77.7 and 79.2 m depth (Fig. 9b).

Microscopic sedimentary facies of the deep distal basin

Thin-sections reveal that the sediment is composed entirely of terrigenous material. No diatoms are visible except in the upper 6 cm (Perren et al. 2003). Detrital organic fragments from higher plants are sometimes present, but are scarce. The laminated nature of the sediment is clearly visible as most contacts between the lithological units are sharp according to the nomenclature of Schnurrenberger et al. (2003). The grain-size of the sediment is clay-silt with traces of sand. At South Sawtooth Lake, laminae assemblages are made of a combination of up to six basic sedimentary facies that are described below and illustrated in Fig. 10. Detailed grain-size measurements using image analysis techniques on the images of Fig. 10 are compiled in Table 1.

Facies 1: silt layers

The coarse silt layer grades into a pure clay-rich layer (Fig. 10a). Each layer conformably lies on top of the clay cap (see below) from the underlying lamina. No erosional features are observed. These layers fine upwards and are composed of fine to medium silts, moderately sorted according to Folk and Ward's nomenclature (1957) (Table 1). Some of the silt layers are so thin (Fig. 11a), that it is impossible to decipher whether they are graded.

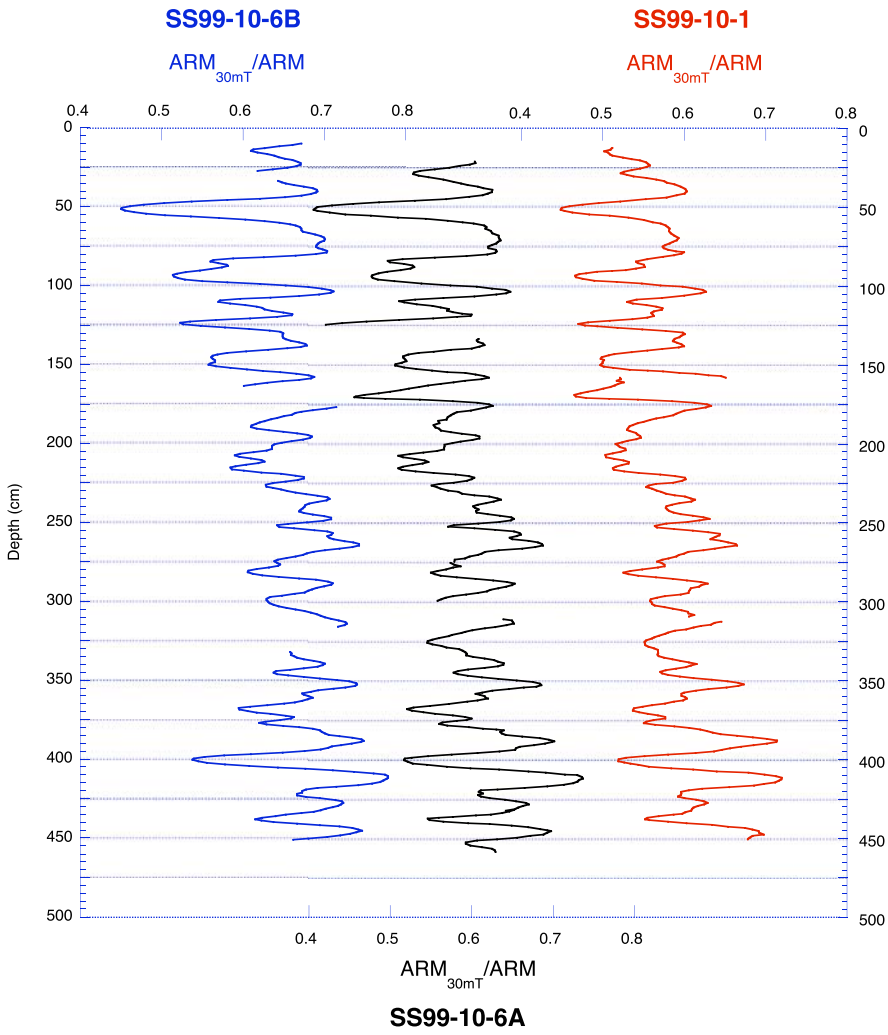

Fig. 8 ARM measured after 30 mT peak AF demagnetization normalized by the ARM on u-channel samples measured at 1-cm spacing from three 4.5-m long vibracores from three locations of the distal basin. Assuming a magnetite dominated magnetic mineralogy ARM_{30mT}/ARM is a proxy for magnetic grain-size with lower values indicating coarser magnetic grain-size, and higher values indicating a finer magnetic grain-size (e.g., Stoner and St-Onge 2007). Though measured at 1-cm spacing, because the width at half height of the magnetometers response function for a u-channel measurement is $\sim$ 4.5 cm these data are smoothed by a similar amount. The difference in values reflects differences in the UC Davis and University of Florida systems. Similarities indicates a strong correlation between the three cores at low resolution. Core locations are shown in Fig. 1

Facies 2: clay caps

Clay caps are composed of clay-sized particles appearing as uniform light gray areas in SEM backscattered images (Fig. 10a). In our thin-sections, clay caps are often outlined by wavy horizontal cracks that are formed when the sediments are freeze-dried during thin-section preparation. Clay cap thickness ranges from a few tens of microns (Fig 10a) to 1 mm (Fig. 10c). Clay caps overlie the other sedimentary facies described above and below, and display a sharp upper contact. Note that grain-size measurements from image analysis techniques are not possible because clay particles are too small (Soreghan and Francus 2004).

Facies 3: sand laminae

Coarser sand laminae occasionally interrupt the regular pattern of sedimentation, but no evidence of erosion is visible under the sand (Figs. 10b and 11b). The grains are not rounded, their median size is usually in the very coarse silt to very fine sand range, and they are typically poorly sorted (see also Table 1). These laminae are usually deposited on top of the silt layer and below the clay cap, but occasionally lie directly on top of the previous lamination's clay cap. These sand layers (Fig. 10b) have a median thickness of 0.5 mm (minimum 0.1 mm; maximum 13 mm). The grain-size of the example presented in Fig. 10 is on the lower end of

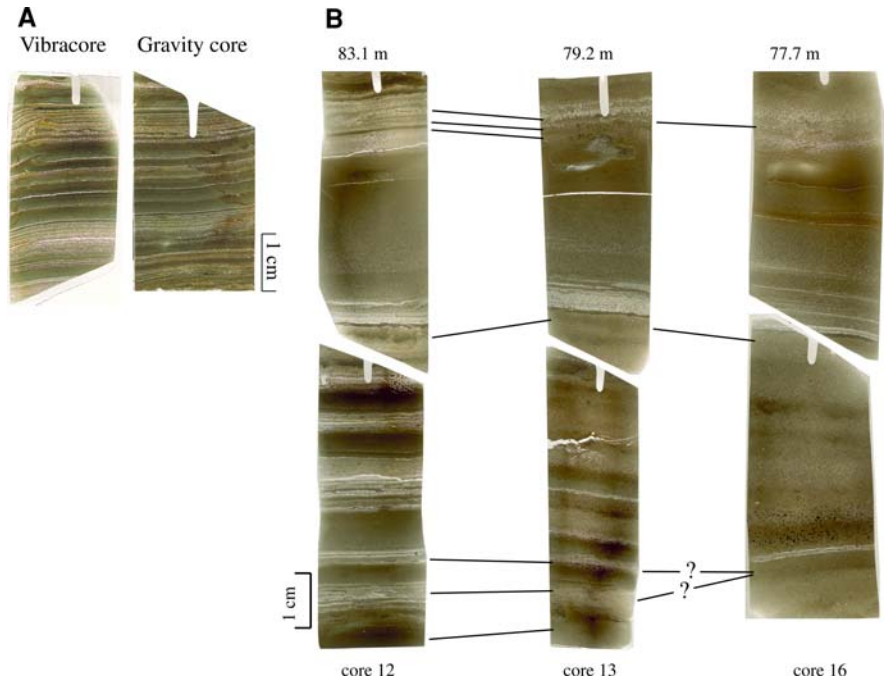

Fig. 9 Flat bed scans of thin-sections in plain light. Vertical groove at the top of the thin-section is a saw mark used for orientation purpose. Lower and/or upper boundaries were cut at an angle to ensure the continuity of the stratigraphic record. (**a**) Example of the excellent stratigraphic match between two cores from the deep distal basin: flat bed scans of two thin-sections from vibracore 10-6B (left) and from gravity core 10-5 (right). Depths below sediment surface are 26.8–31 cm for the thin-sections from vibracores and 33–37 cm for the thin-sections from gravity cores. The stratigraphy of the two cores is almost identical except for slight disturbances due to coring or the making of the thin-section. Images have not been digitally stretched or edited to improve the match. (**b**) Flatbed scans of six thin-sections from the upper part of three short gravity cores in the distal basin along depth gradient. Water depths at which the cores were taken are indicated at the top of each thin-section pair, the deepest one being at the deepest location in the distal basin (see Fig. 1 for location). The black horizontal lines indicate proposed stratigraphic correlations. Fine laminae visible in the deepest pair of thin-sections blur away as the water depth decreases

Fig. 10 Multiscale views of the sedimentary facies of South Sawtooth Lake. Images were digitally enhanced to show sedimentary details. Upper left panel is a macroscopic view of a 15-cm-long section from a vibracore of the distal basin. The scale on the left side is in centimeters. Inset indicates the location of the thin-sections. Just to the right is a flat bed scan of a thin-section acquired in crossed-polarized light using the method outlined in Lamoureux and Bollmann (2004). Dark blue horizontal cracks are due to the making of the thin-section using the freeze-drying method. Vertical groove at the top of the thin-section is a saw mark for orientation. This scan reveals the light colored coarser detrital layers, mostly made of quartz grains. Insets indicate the location of the SEM views. Panels a, b, and d are digital images (2,048 × 1,536 pixels) acquired using a Zeiss EVO XVP 50 SEM in backscattered mode (Soreghan and Francus 2004). Panel c is 1,855 × 3,899 pixels wide. Scale bars are 500 µm. Sedimentary facies presented here are representative of average facies. Results of the measurements performed on these images using image analysis techniques are given in Table 1. (**a**) Clay caps and silt layers. Medium silts (MS) grades up into a pure clay cap (CC). This lamina is 900 µm thick and lies conformably on top of the previous clay cap. No erosional feature is visible. Note some wavy cracks in the CC are formed during the preparation of the thin-sections, and the base of following coarse silt (CS) layer. (**b**) Sand laminae. A layer rich in fine sand is located between a MS and a CC. Most sand grains are angular. (**c**) Graded beds. Photomosaic of a 7-mm-thick graded bed lying on the top of MS. The graded bed is grain supported, moderately well sorted and lies conformably on top of a silt layer. No erosion features are visible. The MS lies conformably on top of the previous CC. A sharp crack (in black) due to freeze drying used during the impregnation separates the silt layer from the previous CC, but no internal disturbance of the sedimentary fabric is visible, except the already mentioned wavy cracks in the clay cap. Isolated sand grains (DS) (facies 5) are visible in the fine silt part of this graded bed. (**d**) Disturbed bed. Two diffuse fine silt layers (Sil) are visible, but lamination limits are barely visible, except for the uppermost CC. Very fine sand and very coarse silt grains are spread across the entire facies (Table 1). On top of this bed, is the base of next year's graded bed with CS ▶

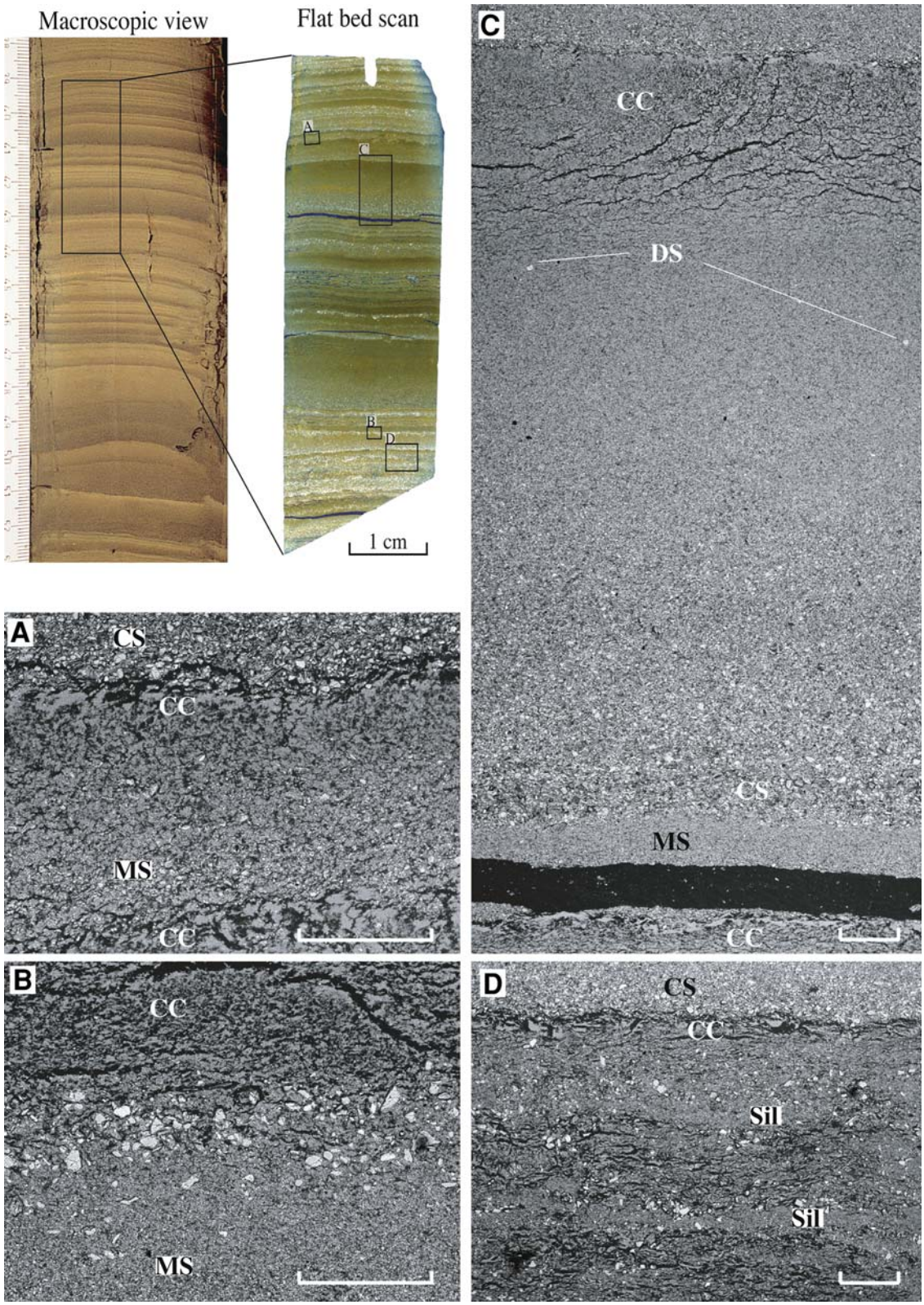
Macroscopic view
Flat bed scan
A
C
B
D
1 cm
C
CC
DS
CS
MS
CC
A
CS
CC
MS
CC
B
CC
MS
D
CS
CC
Sil
Sil

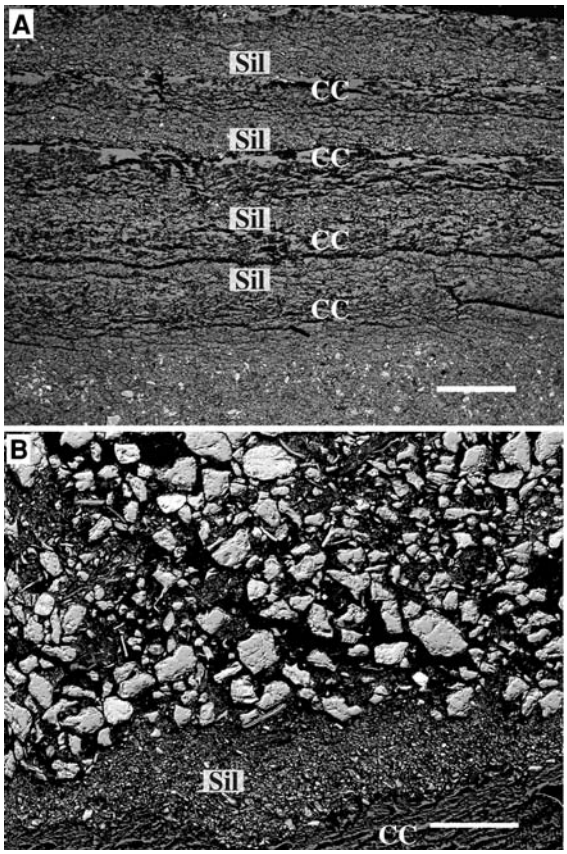

Fig. 11 SEM image in backscattered mode of additional facies not included in the thin-section of Fig. 10. (**a**) Series of very well preserved 500-μm thick laminae, with a succession of silt layers (Sil) and CC. Image is 2,048 × 1,536 pixels, scale bar is 500 μm. (**b**) Base of a coarse grained sand lamina on top of a medium silt layer. This bed corresponds to facies 3 but with coarser grains and grain supported matrix. Image is 1,280 × 960 pixels, scale bar is 200 μm

the size range determined for this facies. Sand laminae with grain-supported fine sand are frequent (Fig. 11b).

Facies 4: graded beds

Thicker graded beds may also interrupt the regular pattern of sedimentation. These usually lie in the identical stratigraphic position as the facies 3 coarse sands (Fig. 10c). A close examination of the contact between the graded beds lying on the initial silt layer reveals two successive grain-size decreases in both units. No reverse grading is observed in the lower unit. Graded beds are usually thicker, with a median thickness of 2.2 mm (maximum: 39 mm). The mean grain-size measured using image analysis techniques at the base of a typical graded bed was 21 μm (Table 1). These thicker graded beds sometimes lie directly on top of the previous clay cap, forming a much thicker lamina compared to facies 1 described above. In rare cases, multiple graded beds occur between two clay caps.

Facies 5: isolated grains

Isolated very coarse silt to very fine sand grains occur within the upper part of graded beds or within the clay caps themselves. These are single grains, the size of which is always much coarser than the surrounding matrix, such as the grains illustrated in Fig. 10c. Alternatively, a few scattered grains may be more or less aligned at the same stratigraphic level.

Facies 6: disturbed beds

Some laminae are disturbed to the point that their boundaries are vague and difficult to distinguish. Those are often a mix of a fine sediment matrix (from clays to medium silts) and coarse silt/sand grains (Fig. 10d), but a clay-rich interval is often visible. The basic sedimentary facies that compose them are difficult to identify.

Laminae assemblages

In summary, the laminated sediments are characterized by the succession of a basic sedimentary facies overlain by a clay cap, with the exception of some disturbed beds. Couplets made of a silt layer and a clay cap are the most common laminae assemblages and are usually well preserved. Their median thickness is 0.9 mm. About a quarter of the laminated structures are triplets made of facies 1 and 2 and an additional facies (#3, 4, or 5). A few laminae assemblages are characterized by multiple laminae (>3) of the same or of a different kind. On rare occasions, couplets are composed of a sand lamina overlaid by a clay cap or a graded bed with a clay cap. Graded beds occur within ~5% of the laminae assemblages.

Discussion

Physical limnology

Physical processes in lakes act as filters between external forcing, like the climate, and the

paleolimnological record (Cohen 2003). In the case of South Sawtooth Lake, limnological characteristics such as the lake ice, density stratification, and dissolved oxygen content can potentially affect the transport and deposition of sedimentary particles, the preservation of the sediments and the distribution of sediment types around the lake basin.

South Sawtooth Lake temperature profiles through the year depict a deep cold monomictic lake (Wetzel 2001): the water column is stratified during the long period when the lake is ice-covered, and then lake water circulates during a short period in summer starting in mid-August. The water column below a depth of 50 m in the distal basin is characterized by different physical properties: homogeneously warmer temperatures (2.2°C), decreasing dissolved oxygen and increasing salinity, leading to a small increase in water potential density (Figs. 5 and 6). As lake ice melted, the water column became over-saturated with oxygen. However, the lowest few meters remained depleted compared to the rest of the water column. We hypothesize that, despite the oligotrophic status of the lake, the long period of ice-cover seals the water body from the atmosphere, allowing biota within the lake to gradually consume oxygen by oxidation of organic matter and respiration (Ellis and Stefan 1989; Wetzel 2001). Eventually, this phenomenon can produce anoxic conditions in water bodies covered by ice for prolonged periods (Golosov et al. 2007). Concomitant to this oxygen depletion, our profiling instruments documented an increase in salinity of about 20 mg l^{-1} in the hypolimnion of the distal basin. Perren et al. (2003) (Table 1) reported concentrations of hypolimnetic dissolved cations in the distal basin, such as Ca^{++}, Mg^{++}, and Si^{++} of about 7.4 mg l^{-1} for the measured cations, which is an enrichment of a similar magnitude. These concentrations were significantly higher than concentrations in the proximal basin and the epilimnion of the distal basin. Because the deep distal basin is the only location within the lake where this increase of cation concentration is observed, it is reasonable to infer that (1) the entire proximal basin and the epilimnion of the distal basin are kept fresh because they receive the bulk of the fluvial input, and that (2) the source of these cations is the sediment itself. Indeed, diffusion rates for many substances are generally low in oxic conditions, but increase significantly under anoxic conditions (Håkanson 2005). Therefore the increase of conductivity might be the result of the low oxygen content in the distal basin. However, little is known about potential mechanisms or processes that are able to release these cations from the sediment to the water body in oligotrophic environments like this one (C. Gobeil and A. Tessier, personal communication, 2007). Other mechanisms for increasing cation concentrations include ground water and freeze out of salts from the ice cover (Stewart and Platford 1986). The former is unlikely because of the presence of permafrost, but the latter needs to be considered. Enrichment from marine water brines (Pagé et al. 1984) is not a factor at South Sawtooth Lake because it is located well above the marine limit. Hence, more investigation is needed to explain this increase of cations at the bottom of the deep distal basin. Also, the water potential density anomaly (σ_θ) increases in the distal basin around 60 m depth, which corresponds to the depth of the sill separating the proximal from the distal basin.

Sediments in the deep distal basin are protected from wind-generated mixing during brief periods of ice-free conditions, and are protected from bioturbation by the anoxic conditions, thus favoring the preservation of very fine laminae. The increases of SSC around JD 155 (4 June) and JD165 (14 June) in 1998 (Fig. 7c) detected at the very bottom of the deep distal basin are difficult to explain in this context and might simply be the result of the SeaCat hitting the lake bottom, causing resuspension of sediment. However, the SSC increase during the JD 161–170 (10–19 June) period corresponds to a period of rainfall (Fig. 4) raising the still unverified hypothesis that the underflow was related to the rainfall event.

Finally, in the context of a warming Arctic and its potential impact on the physical limnology of lakes, it is worth mentioning that the bottom temperatures increased from 2.4 in 1998 to 2.6°C in 2000, and 3.1°C in 2006 (Fig. 5), though the latter measurement was later in the season.

Annually laminated sediments

We focus our efforts on understanding the formation of the finely laminated sediments in the distal basin because these deposits have the potential to contain an undisturbed, annually laminated record valuable for paleoclimate reconstructions. Sediment traps were deployed in 1998 and 1999, but unfortunately, several

attempts to recover them failed. Our previous work (Francus et al. 2002; Perren et al. 2003) briefly presented evidence that laminae at South Sawtooth Lake are annual, and pertinent results are briefly summarized below. Francus et al. (2002) reported the presence of coarse to fine silt layers overlain by a distinctive clay layer, which resulted from the deposition during the winter. They also reported that one additional lamina was present in cores collected in 2000 relative to cores recovered in 1999 and that a ^{137}Cs peak was located at the level of the laminae corresponding to AD 1963 (Francus et al. 2002). Perren et al. (2003) reported that the ^{210}Pb profile appeared diluted by old Pb transported from the watershed, because it oscillates with lamina thickness. However, the constant rate of supply model produced a date of AD 1964, at the depth of the ^{137}Cs peak.

These lines of evidence support the interpretation presented below that the laminae at Sawtooth Lake are formed annually.

Sediment formation

We now interpret the various sedimentary facies based on our detailed microscopic observations in light of the observations made about the physical limnology.

Facies 1: silt layers

Facies 1 is interpreted as being the result of sediment input from snowmelt. During the first week of sustained meltwater flow, and despite the high discharge, the river was not heavily loaded with sediment. The ice-armored ground and frozen river banks protected the sediment from erosion and inhibited the river from transporting a substantial amount of clastic sediment to the lake basin during the initial slush flows (Church and Miles 1982). The result is a cold stream (0 to 0.3°C) with low concentrations of suspended sediments entering the lake where temperature is almost 2°C higher. This thermal contrast produces overflow conditions (Patridge 1999; Sturm and Matter 1978). The sediment transported by the overflows reaches the distal basin, but these conditions are relatively short-lived. Once in the distal basin, the sediment load settles rapidly, as seen in the SSC profiles (Fig. 7). Despite the fact that these overflows do not have a high concentration of sediment, they efficiently disperse a significant amount of the total sediment yield. In 1998, 28% of total SSC transported by the river occurred before JD162 (11 June; Fig. 4), a period that only experienced overflows. Overflows can produce regular graded beds, from silt to clay size, as seen in the thin-section (Fig. 10a). No erosional features are visible. Francus et al. (2002) have shown that the grain size of these silt graded beds are linked to the snowmelt intensity. Similar sedimentary facies have been reported elsewhere in the Arctic (Zolitschka 1996; Moore et al. 2001). Being the lowermost stratigraphic unit in the varve, they represent the spring component of the classic facies of clastic varves (Sturm 1979; O' Sullivan 1983; Zolitschka 2007).

Facies 2: clay caps

According to Stokes' Law, clay-sized particles need a significant amount of time to descend through 80 m of water. Coarse grains are deposited rapidly, and the remaining clay-sized material slowly settles from suspension during ice-covered winter months (Lamoureux 1999). Regardless of the number of sediment pulses that enter the lake during summer, one clay cap forms each year (Sturm 1979). The clay caps are reported elsewhere in Arctic siliciclastic environments as pacing the yearly sedimentation (e.g., Moore et al. 2001; Lamoureux 1999; Zolitschka 1996; Lamoureux and Bradley 1996). The succession of a silt layer followed by a clay cap is the classic mode of varve formation (e.g., O'Sullivan 1983; Zolitschka 2007).

Facies 3: sand laminae

These coarse non-erosive episodes pose a hydrodynamic challenge because the coarse sand grains lie in a fine silt-clay matrix. The coarse sand grains cannot be derived from the river because their size precludes their transport over the 60-m deep sill by the interflows revealed by the SeaCat profiles (Fig. 7b). It is unlikely that the grains are eolian deposits trapped on the lake ice and then dropped in the distal basin at the end of the season when the lake ice melts. Indeed, these sand layers can be anomalously thick and grain-supported (Fig. 11b) and are found in

several cores across the deep distal basin. If the layers were indeed from an eolian or lake-ice source, one would expect them to be more diffuse and have a more patchy distribution across the basin. Significant eolian sediment transport was reported during winter on the Fosheim Peninsula (Lewkowicz 1998), but occurrences of massive sand layers in Arctic sediments have generally only been found in areas in the proximity of large sources of sand like sandurs (Gilbert 2000; Lewis et al. 2002). There is no such source of sand in the South Sawtooth Lake area (Lewis et al. 2002), and the watershed is one of the most vegetated in the High Arctic. We have not observed sand dunes on the ice or sand during our visits in 1998–2000. The fact that these sand layers sometimes occur directly on top of the previous year's clay cap, points to a phenomenon that can take place relatively early in the season, so a source from melting ice is unlikely because complete melting of the lake ice does not typically occur until mid-August. Finally, many attempts to date the sediment using thermoluminescence on different sedimentary facies and size fractions, including the sand fraction, yielded ages that were older than the last glacial period (Forman, University of Illinois, and Wintle, University Aberystwyth, unpublished data), indicating that the sediment was never completely reset with light as it should be in the case of an eolian origin.

We interpret these sand layers as being produced by density flows triggered by events localized in the distal basin or its surroundings. The absence of grading in these sedimentary units eliminates the possibility that turbidity currents transported the material. Most of these sand layers, such as the one illustrated in Fig. 11b, are probably the result of hyper-concentrated density flows according to the classification of Mulder and Alexander (2001). In the water column, these flows move along the slopes of the distal basin and therefore, are not seen in the transmissivity profiles from the central part of the basin, except maybe for the period around JD 165 (14 June). The kind of events responsible for these sand layers remains less clear. Redistribution of shore sediments or subaqueous slumps (Håkanson and Jansson 1983) are potential mechanisms for the frequent deposition of sand layers in the distal basin. However, according to the bathymetry and our observations in the field, a littoral zone does not exist or is poorly developed at the south-western side of the distal basin limiting the amount of sediments available as a source of these deposits. Wind-induced instabilities by wave action are probably limited because ice covers the lake for 10–12 months per year.

Hillslope processes triggered by summer rain events are another possibility. In cold regions, gullying and mass movements are the main processes supplying sediments to the bottom of slopes because they are intensified by the presence of permafrost (Woo and McCann 1994). Occasional large storms can cause severe erosion of the thawed active layer (Cogley and McCan 1976). Indeed, erosion is definitively happening at South Sawtooth Lake as aerial debris flows can be found on the south-western slope bordering the distal basin (Fig. 2b). Moreover, we observed in the field heavily sediment-laden streamlets and gullies on the slopes nearby the lake and entering the distal basin after only a few days of drizzle. In 1998, 5 days of precipitation totaling 32 mm of rain were recorded between JD 161 and JD 165. The concomitant increase of SSC at the bottom of the distal basin may just be due to the SeaCat hitting the lake bottom, but it is also tempting to link this increase with rainfall. However, these observations seem to be in contradiction to the ones drawn elsewhere in the Arctic, which suggest that rainfall of modest intensity appears to have a more limited effect on sediment yield (Cook 1967). According to Lamoureux (2000), there is an effective minimum rainfall that is necessary to generate substantial rain-induced sediment transport. We suggest that the geomorphic and morphologic setting of South Sawtooth Lake and the surrounding slopes explains part of this apparent contradiction. First, the lake is surrounded by steep slopes exposed to hillslope processes that are not present at Nicolay Lake (Lamoureux 2000). Second, the watershed of South Sawtooth Lake is located in the col of the Sawtooth Mountains range, and recorded twice the amount of rain recorded at Eureka, located at sea level, during the period for which we have parallel measurements (Lewis et al. 2002). Precipitation for June and July 1994 at a nearby site in the Sawtooth Range totaled 64 mm, an amount equal to the mean annual value at Eureka (Lewkowicz and Hartshorn 1998). Moreover, sediment transfer at South Sawtooth Lake seems very sensitive to summer rainfall events. Indeed, Lewis et al. (2005) reported a large sediment pulse in the

river's SSC (SSC reached 83760 mg l^{-1}) with a modest increase of discharge (from 0.4 to 1.2 m^3 s^{-1}) after a small rainfall event (5.2 mm) occurring on July 7th of 1998. Between 25 and 35 mm of rain is believed to have triggered a hillslope debris flow in 1995 in an adjacent valley (Lewkowicz and Hartshorn 1998). These values are far below the normal thresholds for debris flows in permafrost areas (Larson 1982 cited in Lewkowicz and Hartshorn 1998). Still according to Lewkowicz and Hartshorn (1998), "Channelized debris flows have occurred at a fairly constant rate of one high-magnitude debris flow across the slope every 4–5 years." Because of the localized nature of precipitation events in the Canadian High Arctic, and until we have direct evidence from sediment traps to directly link the occurrences of sand layers with rain events recorded by instrumental records, this connection must be considered a working hypothesis. However, we note that similar sand layers were found in Donard Lake, Baffin Island, and extreme rainfall events were among the several interpretations suggested by the authors (cf. Fig. 7 in Moore et al. 2001).

Facies 4: graded beds

Facies 4 is interpreted to be the result of an increase in stream discharge due to pluvial events after the snowmelt peak. Rising temperatures increase the thickness of the active layer, the saturation of soils, and slope instability. Therefore, after the snowmelt peak, discharge events are likely to be more loaded with sediment. For instance, pulses observed on 27 June and 7 July 1998 had high SSC (3,600 and 60,800 mg l^{-1}, respectively: Lewis et al. 2005). On JD162 (11 June), the river temperature became warmer and denser than the temperature of the water in the epilimnion (1.3°C) (Fig. 4) and the relatively warm and heavily sediment-laden flow entering the lake turned into underflows and filled the proximal basin with the coarsest sediment fraction (Fig. 7a).

However, the most turbid events are able to reach the sill between the two basins and spill over into the distal basin as interflows (Fig 7b). Our dataset revealed a significant increase of SSC to 7 mg l^{-1} at a depth of 55 m at site 10 on JD 183 (2 July; Fig. 7b), a few days after a significant increase of the river runoff and SSC (Fig. 4). Only the finest grains are able to reach the distal basin as revealed by the presence of coarse silt at the base of these graded beds (Fig. 10c). Turbulent flow is the most likely process for the transportation of these particles (Mulder and Alexander 2001). Some density stratification that coincides with the depth of the weak chemocline (Fig. 6) remains in the distal basin at ~65 m depth because these turbulent flows are observed to be interflows (Fig. 7). Interflows are recorded over a relatively long time (we observed them for 2 weeks) compared to underflows. Once in the distal basin, the sediment settles to form very regular graded beds without visible erosional features. The maximum grain-size of these graded beds is likely to be controlled by the intensity of the turbulent flow entering the distal basin. Our data are not sufficient to assess whether it is the maximum discharge of the river during the pluvial events that controls the turbidity of these flows. The thickness of the graded beds is likely to be controlled by the amount of fine particles transported by the turbulent interflows and their duration, or the effectiveness of this dispersal mechanism (Smith and Ashley 1985). Multiple graded beds are sometimes observed between two clay caps indicating that these events are relatively short-lived compared to the period of annual sedimentation. Because they can be very thick (up to 39 mm), this process is a major contributor to the sediment deposition in the distal basin. Some coarse sand layers (facies 3) may interrupt the grading, reinforcing the argument that completely different mechanisms are responsible for the formation of these two different facies. The graded beds usually lie on top of the fine silt layers (Fig. 10c). The underlying silt layers always display a normal grading, ruling out the possibility of being the signature of waxing flows (rising limb of the flows) that usually lead to the deposition of inversely graded beds (Mulder et al. 2001). When a graded bed directly lies on the top of a clay cap, it is very difficult to distinguish whether it was deposited by an overflow or an interflow, although the basal silt grain size of these graded beds seems to be significantly larger (coarse silt) (Table 1—facies 4 graded bed lower half; mean diameter = 21.2 μm) compared to the grain size of facies 1 silt layers (medium silt) (Table 1—facies 1; mean diameter = 9.3 μm). The quality of sorting might provide some answers but this requires additional measurements (Table 1) to be conclusive. Lamoureux and Bradley (1996),

Lamoureux (2000), and Hambley and Lamoureux (2006) reported similar facies in other Arctic lakes and linked their occurrence with pluvial events. In brief, there is a strong set of facts that suggests that these facies are probably caused by rain events that trigger a significant increase in river discharge and sediment transport, although it still needs to be confirmed by sediment trapping and/or correlations with long-term climate data.

Facies 5: isolated grains

Isolated coarse grains are clasts that pose a hydrodynamic paradox because the energy needed to transport them laterally is higher than that necessary to deposit the hosting sediment (Bennett et al. 1996). In Arctic lakes, one obvious mechanism for such deposits is from wind-blown grains on the frozen lake that settle when the ice cover melts. Such deposits have been reported in many northern lake sediments (Retelle 1986; Lamoureux 1999; Lewis et al. 2002; Lamoureux and Gilbert 2004). At South Sawtooth Lake, this interpretation is supported by the fact that the sands grains are always found within the upper part of graded beds or within the clay caps, which point to a deposition after the main sediment input period. As stated previously, there is no significant source of eolian material surrounding South Sawtooth Lake such as proximal sandurs (Lamoureux et al. 2002; Gilbert 2000). This is consistent with the rare occurrence of isolated grains (less than 5% of the varves).

Facies 6: disturbed beds

Disturbed beds are difficult to interpret because their boundaries are unclear. They are usually a mix of very fine particles and coarser grains. The first hypothesis that could explain their formation is that some coarse sand grains brought into the center of the distal basin by hyperconcentrated density flows sink into a poorly consolidated clay-rich matrix. If this hypothesis is correct, the mechanism responsible for this facies is similar to that of loadcasts (Reineck and Singh 1986). It is not clear whether the flow itself can also produce some disturbance (T. Mulder, personal communication; Mulder and Alexander 2001). The second interpretation is that some bioturbation occurs occasionally at the very bottom of the distal basin. Figure 9b shows that laminae tend to have blurred boundaries as depth decreases. In our core transect, overall lamination thickness does not seem to decrease away from the deepest location. This rules out the possibility that sediment focusing in the deepest part of the basin prevents bioturbation from taking place because of a higher sedimentation rate, though the variation of oxygen content in the deeper part of the distal basin might be a factor. Indeed, at the beginning of the season, the amount of dissolved oxygen in the water column is about 6 mg l^{-1}, with the lowermost few meters being more depleted—down to 4.6 mg l^{-1}, with a concomitant increase of salinity (0.05–0.08 ppt). Dissolved oxygen concentrations are >2.5 mg l^{-1}, too high to induce fish mortality (Ellis and Stefan 1989) or to prevent fish and other organisms from living in this zone. However, habitat change is a very common behavioral response when spatial heterogeneity permits fish to select dissolved oxygen availability by moving (Kramer 1987). A profile measured at the end of August, 2006 showed that the water column was saturated with dissolved oxygen except for the lowermost 2 m, with values down to 4.8 mg l^{-1} (Fig. 6b). If mixing of the water column occurs completely when the ice-free period is longer and/or because wind intensity is stronger, then it might be possible for the lake's lowermost water to become oxygen-saturated for at least a short period of time (Ohlendorf et al. 2000), favoring organisms that may disturb the sediment. The occurrence of disturbed sediment might therefore be linked to the duration of ice-cover and hence to summer temperature, although this hypothesis needs to be confirmed by long-term monitoring. The hypothesis that bioturbation is responsible for disturbance of these beds is strengthened by grain-size measurements. Indeed the characteristics of the grain-size distribution of the disturbed facies illustrated in Fig. 10d and Table 1 are quite similar to those of the sand layer facies (Fig. 10b, Table 1). In this particular case, one can hypothesize that our disturbed facies is the result of the bioturbation of the rain event facies illustrated here. Perturbation due to load casts would probably mix sediment with different grain-size characteristics. This observation also needs to be verified by additional measurements (Fig. 10) to be conclusive. Finally, we note that the uppermost layers at South Sawtooth Lake belong to facies 6 and this corresponds to the appearance of diatoms in the sediment record after several thousand

years without their presence in the sediment (Perren et al. 2003). Alternatively, the relationship might not be straightforward since a decrease of the oxygen content could result from degradation of organic matter. An increase in lake productivity due to warming will also produce more organic matter to be degraded, perhaps leading to more intense anoxic conditions.

In short, it is difficult to conclude for certain that bioturbation is responsible for the disturbed beds although multiple lines of evidence point to disturbance by benthic activity.

Quality of the distal basin sequence for paleoclimate reconstruction

Our quest to understand sediment formation at South Sawtooth Lake was also driven by the need to assess the quality of the paleoclimatic record to be reconstructed for this site. The continuity of the sequence is illustrated by the fact that correlations between cores are very easy to perform macroscopically and microscopically (Fig. 9a). The profiles of magnetic properties, from long cores taken at different locations in the lake are strikingly similar (Fig. 8) and confirm that the sequences are continuous and complete at low resolution. The interpretations of the six sedimentary facies from the distal basin described above rule out the possibility of major erosional events: erosion from turbidity flows initiated by high river discharge is unlikely because of the presence of the sill, though it is not known whether hyperconcentrated density flows produce local erosion (T. Mulder, personal communication). The internal structure of the laminae contains evidence of annual cyclicity. SEM views of the laminae in backscattered mode make it possible to measure and analyze sedimentary structure in very fine laminae down to 400 μm thickness (Fig. 11) that are not visible with other techniques. We argue that if such fine laminae are present, lamination preservation is excellent at this site. However, even though we were able to distinguish laminae as thin as 400 μm, one cannot rule out the possibility of having years with very little snowfall or snowmelt, no lake ice melting and/or no input from summer precipitation, and hence no recordable sedimentation. It is conceivable that in the coldest years of the Little Ice Age there may have been some years without sedimentary input to South Sawtooth Lake. In any case, our work demonstrates the need for studying Arctic detrital laminated records with thin-sections in order to establish a complete chronology.

General discussion

Our study has outlined the complexity of processes driving the formation of the sedimentary structures in South Sawtooth Lake. Varves that form in snowmelt-fed Arctic environments are the sum of complex interactions of several processes, and varve thickness alone should not be used for hydroclimatic reconstructions. This echoes the conclusions made from glaciolacustrine sequences (Bradley et al. 1996; Hodder et al. 2007) that multidisciplinary and systemic approaches are needed to understand varves as hydroclimatic proxies. Our detailed sedimentological description, combined with limnological and hydroclimatic observations provides information about the processes driving the formation of the varves. However, the data presented here are only a snapshot and may not provide a comprehensive view of the hydroclimatic, limnological, and sedimentological systems at South Sawtooth Lake. Still, these data are valuable because so little information is known about sedimentary processes in High Arctic lakes, and they enrich our understanding of the processes occurring in these systems. The evidence presented here reinforces the interpretation of the sedimentary processes in Francus et al. (2002) and the basis for the chronology provided by Francus et al. (2002) and Perren et al. (2003). More specifically, the relation between silt layers grading into clay layers with early snowmelt has been confirmed by our analyses of sediment microstructure. However, the on-site precipitation record is short and precludes us from definitively concluding that the sand layers and the graded layers are linked to rain events. This is a clear indication that long-term monitoring of lakes and their watersheds is essential to build a strong model for hydroclimatic proxies (Hodder et al. 2007), despite the complicated logistics.

Conclusions and summary

Based on observations of hydrology, physical limnology, and micro-sedimentology, we demonstrated that laminated sediments in the distal basin of South

Sawtooth Lake display classic features of clastic varves (Zolitschka 2007). The most important part of the sediment—thin graded medium silt layers—is caused by the settling in the water column of sediments that were transported by overflows triggered by early season snow melt. The detailed description of sediment fabric confirms the evidence presented in Francus et al. (2002) that the grain-size of these layer is correlated to processes related to snowmelt. Sand layers interrupt this low-energy, relatively slow sedimentation process. These are probably due to hyperconcentrated density flows that have been initiated within the distal basin. Our best interpretation of the triggering mechanism is summer rain events eroding the active layer on the steep hills and transport along gullies to the lake, although this is not yet proven by a calibration against the weather record. Graded beds also interrupt the regular pattern of sedimentation and are deposited by turbulent flows that travel across the proximal basin and reach the distal basin as interflows, releasing their sediment load to the lake floor below by suspension settling. Finally, disturbed beds are likely to be due to bioturbation. Our evidence suggests that the sequence in the deepest portion of the distal basin is continuous, without significant erosion. Even though the possibility of years without any sedimentation cannot be ruled out, our observations strongly imply that the sediment record is undisturbed and continuous at South Sawtooth Lake and that the accumulation of sediment, at least in the distal basin, is spatially uniform (Petterson et al. 1993). Our understanding of the processes leading to the deposition of the sediment thus provides the necessary basis for retrieving a high quality paleoclimate reconstruction from this site.

Acknowledgments Part of this work is based on Whitney Patridge's bachelor degree thesis (Bates College, 1999). We thank Jacques Labrie and Frank Keimig for their support in figure drawing and data processing. We also thank Mark Besonen, Carsten Braun, Tim Cook, Doug Hardy, Whitney Patridge, Bianca Perren, and Mindy Zapp for their help in the field. We also thank the Polar Continental Shelf Project for efficient logistic support. A. Tessier, C. Gobeil, and T. Mulder provided helpful insights regarding specific aspects of the paper. This work was made possible thanks to NSF awards ATM-9708071 and ATM-040242 to the University of Massachusetts, and to NSERC discovery and northern supplement grants to Pierre Francus. This is Polar Continental Shelf Project contribution # 047-07.

References

Bell T (1996) The last glaciation and sea level history of Fosheim peninsula, Ellesmere Island, Canadian High Arctic. Can J Earth Sci 33:1075–1086

Bennett MR, Doyle P, Mather AE (1996) Dropstones: their origin and significance. Palaeogeogr Palaeoclimatol Palaeoecol 121:331–339

Blass A, Bigler C, Grosjean M, Sturm M (2007) Decadal-scale autumn temperature reconstruction back to AD 1580 inferred from the varved sediments of Lake Silvaplana (southeastern Swiss Alps). Quat Res 68:184–195

Blott SJ, Pye K (2001) Gradistat: a grain size distribution and statistics package for the analysis of unconsolidated sediments. Earth Surf Process Landforms 26:1237–1248

Bradley RS, Retelle MJ, Ludlam SD, Hardy DR, Zolitschka B, Lamoureux SF, Douglas MSV (1996) The Taconite Inlet Lakes project: a systems approach to paleoclimatic reconstruction. J Paleolimnol 16:97–110

Braun C, Hardy DR, Bradley RS, Retelle MJ (2000) Streamflow and suspended sediment transfer to Lake Sophia, Cornwallis Island, Nunavut, Canada. Arct Antarct Alp Res 32:456–465

Church M, Miles M (1982) Processes and mechanisms of river bank erosion. In: Hey RD, Bathurst JC, Thorne CR (eds) Gravel-bed rivers: fluvial processes, engineering, and management. Wiley, New York, pp 259–271

Cogley JG, Mc Cann SB (1976) An exceptional storm and it effects in the Canadian High Arctic. Arct Alp Res 8: 105–110

Cohen AS (2003) Paleolimnology. Oxford University Press, New York

Cook FA (1967) Fluvial processes in the High Arctic. Geogr Bull 9:262–268

Dawes PR, Christie RL (1991) Geomorphic regions. In: Trettin HP (ed) Geology of the innuitian orogen and Arctic Platform of Canada and Greenland. Geological Survey of Canada. Geol Can 3:29–56

Edlund SA, Alt BT (1989) Regional congruence of vegetation and summer climate patterns in the Queen Elizabeth Islands, Northwest Territories, Canada. Arctic 42:3–23

Ellis CR, Stefan HG (1989) Oxygen-demand in ice covered lakes as it pertains to winter aeration. Water Resour Bull 25:1169–1176

Environment Canada (2003) Canadian Climate Normals 1971–2000. http://climate.weatheroffice.ec.gc.ca/climate_normals/index_e.html

Folk RL, Ward WC (1957) Brazos River bar: a study in the significance of grain size parameters. J Sediment Petrol 27:3–26

Francus P (1998) An image analysis technique to measure grain-size variation in thin sections of soft clastic sediments. Sediment Geol 121:289–298

Francus P, Asikainen C (2001) Sub-sampling unconsolidated sediments: a solution for the preparation of undisturbed thin-sections from clay-rich sediments. J Paleolimnol 26:323–326

Francus P, Karabanov E (2000) A computer-assisted thin-section study of lake Baikal sediments: a tool for

understanding sedimentary processes and deciphering their climatic signal. Int J Earth Sci 89:260–267
Francus P, Bradley RS, Braun C, Abbott M, Keimig F (2002) Paleoclimate studies of minerogenic sediments using annually resolved textural parameters. Geophys Res Lett 29, 1998. doi:10.1029/2002GL015082
Garneau M, Alt BT (2000) Environmental response to climate change in the Canadian High Arctic. Geological Survey of Canada, Bulletin 529, Ottawa, Canada
Geological Survey of Canada (1972) Geological Map, Cañon Fiord, District of Franklin, Map 1308A, scale 1:250,000
Gilbert R (2000) Environmental assessment from sedimentary record of high-latitude fiords. Geomorphology 32: 295–314
Gilbert R, Butler RD (2004) The physical limnology and sedimentology of Meziadin Lake, northern British Columbia, Canada. Arct Antarct Alp Res 36:33–41
Gilbert R, Desloges JR, Clague JJ (1997) The glacilacustrine sedimentary environment of Bowser Lake in the northern Coast Mountains of British Columbia, Canada. J Paleolimnol 17:331–346
Glew JR, Smol JP, Last WM (2001) Sediment core collection and extrusion. In: Last WM, Smol JP (eds) Tracking environmental change using lake sediments: basin analysis, coring, and chronological techniques, vol 1. Kluwer Academic, Dordrecht, The Netherlands, pp 73–106
Golosov S, Maher O, Schipunova E, Terzhevik A, Zdorovennova G, Kirillin G (2007) Physical background of the development of oxygen depletion in ice-covered lakes. Oecologia 151:331–340
Håkanson L (2005) The importance of lake morphometry for the structure and function of lakes. Int Rev Hydrobiol 90:433–461
Håkanson L, Jansson M (1983) Principle of lake sedimentology. Springer Verlag, Heidelberg, 316 pp
Hambley GW, Lamoureux SF (2006) Recent summer climate recorded in complex varved sediments, Nicolay lake, Cornwall Island, Nunavut, Canada. J Paleolimnol 35:629–640
Hardy DR (1995) Streamflow and sediment transfer from a mountainous high arctic watershed, Northern Ellesmere Island. PhD Thesis. University of Massachusetts, Amherst, MA, 267 pp
Hardy DR (1996) Climatic influences on streamflow and sediment flux into lake C2, northern Ellesmere Island, Canada. J Paleolimnol 16:133–149
Hardy DR, Bradley RS, Zolitschka B (1996) The climatic signal in varved sediments from Lake C2, northern Ellesmere Island, Canada. J Paleolimnol 16:227–238
Hodder KR, Gilbert R, Deslosges JR (2007) Glaciolacustrine varved sediment as an alpine hydroclimatic proxy. J Paleolimnol 38:365–394
JPOTS Editorial Panel (1991) Processing of oceanographic station data. NESCO, Paris, France
Kramer D (1987) Dissolved oxygen and fish behavior. Environ Biol Fish 18:81–92
Lamoureux SF (1994) Embedding unfrozen lake sediments for thin section preparation. J Paleolimnol 10:141–146
Lamoureux SF (1999) Catchment and lake controls over the formation of varves in monomictic Nicolay Lake, Cornwall Island, Nunavut. Can J Earth Sci 36:1533–1546
Lamoureux SF (2000) Five centuries of interannual sediment yield and rainfall induced erosion in the Canadian High Arctic recorded in lacustrine varves. Water Resour Res 36:309–318
Lamoureux SF, Bollmann J (2004) Image acquisition. In: Francus P (ed) Image analysis, sediments and paleoenvironments. Kluwer Academic Publisher, Dordrecht, The Netherlands, pp 11–34
Lamoureux SF, Bradley RS (1996) A late Holocene varved sediment record of environmental change from Northern Ellesmere Island. J Paleolimnol 16:239–255
Lamoureux SF, Gilbert R (2004) A 750-yr record of autumn snowfall and temperature variability and winter storminess recorded in the varved sediments of Bear Lake, Devon Island, Arctic Canada. Quatern Res 61:134–147
Lamoureux SF, Gilbert R, Lewis T (2002) Lacustrine sedimentary environments in High Arctic Proglacial Bear lake, Devon Island, Nunavut, Canada. Arct Antarct Alp Res 34:130–141
Lewis T, Gilbert R, Lamoureux SF (2002) Spatial and temporal changes in sedimentary processes in proglacial Bear Lake, Devon Island, Nunavut, Canada. Arct Antarct Alp Res 34:119–129
Lewis T, Braun C, Hardy DR, Francus P, Bradley RS (2005) An extreme sediment transfer event in a Canadian High Arctic river. Arct Antarct Alp Res 37:477–482
Lewis T, Francus P, Bradley RS (2007) Limnology, sedimentology, and hydrology of a jökulhlaup into a meromictic high arctic lake. Can J Earth Sci 44:791–806
Lewkowicz AG (1998) Aeolian sediment transport during winter, Black Top Creek, Fosheim Peninsula, Ellesmere Island, Canadian Arctic. Permafrost Periglac 9:35–46
Lewkowicz AG, Hartshorn J (1998) Terrestrial record of rapid mass movements in the Sawtooth Range, Ellesmere Island, Northwest Territories, Canada. Can J Earth Sci 35:55–64
Moore JJ, Hughen KA, Miller GH, Overpeck JT (2001) Little Ice Age recorded in summer temperature reconstruction from varved sediments of Donard Lake, Baffin Island, Canada. J Paleolimnol 25:503–517
Mulder T, Alexander J (2001) The physical character of subaqueous sedimentary density flows and their deposits. Sedimentology 48:269–299
Mulder T, Migeon S, Savoye B, Faugères JC (2001) Inversely graded turbidite sequences in the deep Mediterranean: a record of deposits from flood-generated turbidity currents? Geo-Mar Lett 21:86–93
Ó Cofaigh C (1999) Holocene emergence and shoreline delevelling, southern Eureka Sound, High Arctic Canada. Geogr Phys Quatern 53:235–247
Ó Cofaigh C, England J, Zreda M (2000) Late Wisconsinan glaciation of southern Eureka Sound: evidence Innuitian ice in the Canadian High Arctic during the Last Glacial Maximum. Quatern Sci Rev 19:1319–1341
O' Sullivan PE (1983) Annually-laminated lake sediments and the study of Quaternary environmental changes—a review. Quatern Sci Rev 1:245–313
Ohlendorf C, Niessen F, Weissert H (1997) Glacial varve thickness and 127 years of instrumental climate data: a comparison. Clim Change 36:391–411

Olhendorf C, Bigler C, Goudsmit G-H, Lemcke G, Livingstone D, Lotter AF, Müller B, Sturm M (2000) Causes and effects of long periods of ice cover on a remote high Alpine lake. J Limnol 59(Suppl 1):65–80

Pagé P, Ouellet M, Hillaire-Marcel C, Dickman M (1984) Isotopic analyses (^{18}O, ^{13}C, ^{14}C) of two meromictic lakes in the Canadian Arctic Archipelago. Limnol Oceanogr 29:564–573

Patridge WJ (1999) Modern sediment transport and deposition in a High Arctic lacustrine environment; relationship between depositional dynamics and climate. Undergraduate thesis. Bates College, Lewiston, Maine

Perren B, Bradley RS, Francus P (2003) Rapid lacustrine response to recent High Arctic warming: a diatom record from Sawtooth Lake, Ellesmere Island, Nunavut. Arct Antarct Alp Res 35:271–278

Petterson G, Renberg I, Geladi P, Lindberg A, Lindgren F (1993) Spatial uniformity of sediment accumulation in varved lake sediments in northern Sweden. J Paleolimnol 9:195–208

Reineck IB, Singh HE (1986) Depositional sedimentary environments: with reference to terrigenous clastics. Springer Verlag, Berlin

Retelle MJ (1986) Stratigraphy and sedimentology of high arctic coastal lacustrine basins, northeastern Ellesmere Island, northwest Territories. Can Geogr Phys Quatern 40:117–128

Retelle MJ, Child JK (1996) Suspended sediment transport and deposition in a high arctic meromictic lake. J Paleolimnol 16:151–167

Schnurrenberger D, Russell J, Kelts K (2003) Classification of lacustrine sediments based on sedimentary components. J Paleolimnol 29:141–154

Smith ND, Ashley GM (1985) Proglacial lacustrine environment. In: Ashley GM, Shaw J, Smith ND (eds) Glacial sedimentary environments. SEPM, Tulsa, OK, pp 135–216

Smith SV, Bradley RS, Abbott MB (2004) A 300 year record of environmental change from Lake Tuborg, Ellesmere Island, Nunavut, Canada. J Paleolimnol 32:137–148

Soreghan MJ, Francus P (2004) Processing backscattered electron digital images of thin section. In: Francus P (ed) Image analysis, sediments and paleoenvironments. Kluwer Academic Publisher, Dordrecht, The Netherlands, pp 203–225

Stewart KM, Platford RF (1986) Hypersaline gradients in two Canadian High Arctic lakes. Can J Fish Aquat Sci 43:1795–1803

Stoner JS, St-Onge G (2007) Magnetic stratigraphy: reversals, excursions, paleointensity and secular variation. In: Hillaire-Marcel C, de Vernal A (eds) Development in marine geology: volume 1. Proxies in Late-Cenozoic paleoceanography, Elsevier, pp 99–138

Sturm M (1979) Origin and composition of clastic varves. In: Schlüchter C (ed) Moraines and varves. Balkema, Rotterdam, pp 281–285

Sturm M, Matter A (1978) Turbidites and varves in Lake Brienz (Switzerland): deposition of clastic detritus by density. In: Matter A, Tucker ME (eds) Modern and ancient lake sediments. Int Assoc Sedimentol Spec Publ 2:147–168

Wetzel RG (2001) Limnology: lake and river ecosystems, 3rd edn. Academic Press

Zolitschka B (1996) Recent sedimentation in a high arctic lake, northern Ellesmere Island, Canada. J Paleolimnol 16: 169–186

Zolitschka B (2007) Varved lake sediments. In: Elias SA (ed) Encyclopedia of quaternary science. Elsevier, Amsterdam, pp 3105–3114

Woo M, McCann SB (1994) Climatic variability, climate change, runoff, and suspended sediment regimes in northern Canada. Phys Geogr 15:201–226